Electric Field Nuclear Double Resonance in Ag+-Doped NaCl†

W. J. Meyer, * D. V. Lang, ‡ and C. P. Slichter

Department of Physics and Materials Research Laboratory, University of Illinois,
Urbana, Illinois 61801

(Received 5 March 1973)

An electric field-nuclear-magnetic-double-resonance experiment is described which enables the resolution of certain weak resonances otherwise concealed under a nearby, much stronger resonance. In Ag+-doped NaCl, the weak resonance of the nearest-neighbor sodium nuclei to the Ag+ impurity is concealed by the strong resonance of the sodium nuclei far from the impurity due to the small quadrupole splitting of the nearest neighbors. The technique is based on the fact that the Ag+ ion breaks the inversion symmetry of the near neighbors, whereas the distant nuclei remain at sites of inversion symmetry. As a result, an external oscillating electric field can induce $\Delta m = \pm 2$ transitions in the near neighbors but not in the distant ones. The absorption is detected by monitoring the saturation of the magnetic resonance of the distant nuclei as a function of electric field frequency. The nearest-neighbor sodium nuclei were found to have a static quadrupole coupling constant $\nu_Q = 12.5 \pm 0.2$ kHz with an asymmetry parameter of $\eta = 0.28 \pm 0.04$. A simple theory is developed which explains the intensities of the quadrupole lines as a function of the orientation of the electric and magnetic fields. A dynamic quadrupole coupling constant ν_D is defined. For the nearest-neighbor sodium nuclei $\nu_D \sim 3 \times 10^{-2}$ Hz/(V/cm) and for the next-nearest-neighbor sodium nuclei $\nu_D \sim 3 \times 10^{-4}$ Hz/(V/cm).

I. INTRODUCTION

Recently, pulsed nuclear magnetic double resonance (PNMDR) has been used to measure quadrupole splittings of the Zeeman energy levels of nuclei that are near neighbors to substitutional impurities in alkali-halide crystals.[1-5] Mallick and Schumacher[1] and Spencer, Schmid, and Slichter[2] have studied the NaCl system with an Ag+ substitutional impurity. In their studies only the second shell of sodium nuclei, containing the (2, 0, 0) neighbors with respect to the impurity site at (0, 0, 0), was observed and found to have a quadrupole coupling of 40 kHz. The first shell of sodium nuclei, containing the (1, 1, 0) neighbor, was not observed.

Based on the experimental results of Hartland,[5] Nelson and Ohlsen,[3] and the calculations of Dick[6] and Satoh et al.[4] suggested the possibility that the first shell of sodium nuclei may have a smaller quadrupole coupling than the more distant second shell. If that is the situation, the smaller splittings could place the quadrupole lines close enough to or under the main sodium absorption line, so that the small absorption from the first shell would be swamped by the main absorption of the vast majority of sodium nuclei far from the impurity. This can be visualized upon examination of the double-resonance spectra from Spencer et al.[2] in Fig. 1. It is impossible to resolve quadrupole lines residing within 15–20 kHz of the main line absorption centered at ν_0, the Larmor frequency for Na²³. Although the linewidth of the Na²³ resonance is only about 2.3 kHz, PNMDR yields a large absorption even in the tail of the main line. This is a specific example of a general problem encountered in nuclear resonance and a problem dealt with in this paper; it is difficult and sometimes impossible to observe weak resonances from low-abundance nuclei that reside under much stronger resonance of an abundant species.

In this paper an electric field-double-resonance (EFDOR) technique is described which has enabled us to overcome this problem. We report the observation of the quadrupole spectrum of the first shell of sodium nuclei in a NaCl single crystal with 0.5-at.% Ag² doping and verify the hypothesis of Spencer et al. that it *is* concealed by the main line when one uses conventional methods.

The technique is based on an idea first suggested by Bloembergen.[7] He predicted that if the nuclear site lacked inversion symmetry and had a quadrupole moment, spin transitions could be induced by applying a time-varying external electric field to a crystal lattice at a frequency corresponding to resonance between two nuclear-spin levels. He also predicted that transitions of $|\Delta m| > 1$ could be induced. In addition, Armstrong, Bloembergen, and Gill[8] mentioned the possibility of double-resonance experiments in which transitions induced by an external oscillating electric field could be monitored by the magnetic $\Delta m = \pm 1$ transition. These ideas have been demonstrated by Brun, Hann, Pierce, and Tanttila[9] in GaAs; by Luukkala[10] in NaClO₃; and by Kushida and Silver[11] in Al₂O₃.

Our interest arose upon the recognition that these features had special advantages for the defect problem in NaCl:Ag. The success of the experiment
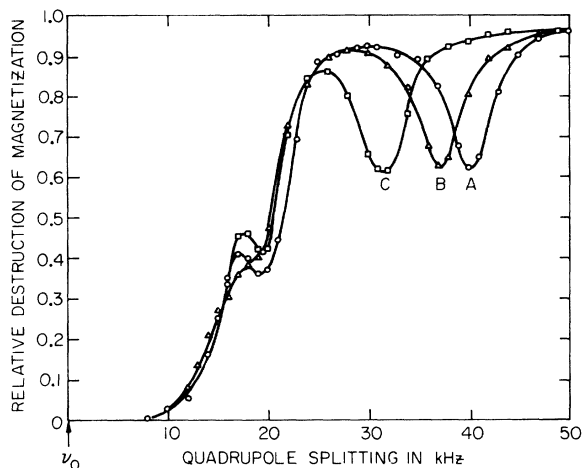
FIG. 1. Nuclear-double-resonance spectra for NaCl single crystal containing 0.1-mole% Ag^+ impurities. The angle between the $\langle 100 \rangle$ direction and the external magnetic field was $0°$, $10°$, and $20°$ for A, B, and C, respectively. ν_0 is the Larmor frequency of the Na^{23} nucleus (after Spencer et $al.$).

presented in this paper hinges on the fact that the sodium nuclei that are near neighbors to the silver impurity are not at sites of inversion symmetry whereas the sodium nuclei far from the impurity are. By applying an electric field at $2\omega_0 + \omega_Q$, where ω_0 is the Larmor frequency of Na^{23} and ω_Q, the quadrupole frequency, spin transitions of $\Delta m = \pm 2$ are induced in the near-neighbor sodium nuclei, but not in the distant ones. $Thus$, a $symmetry$ $selection$ $rule$ has $been$ $invoked$. The absorption of the near-neighbor nuclei is then detected by monitoring the destruction of magnetization of the distant nuclei as a function of electric field frequency. In this manner it is possible to observe a quadrupole splitting which is otherwise obscured by the huge absorption of the main line.

In Sec. II the details of the EFDOR processes are discussed along with the experimental procedure and apparatus. Section III presents theory and experimental results.

II. EXPERIMENT

A. Detailed Explanation of the EFDOR Process in NaCl : Ag

The abundant nuclei, those sodium nuclei far from the impurity, are at sites of cubic symmetry and thus the electric field gradients (EFG's) are zero. They are also at sites of inversion symmetry. Since $I = \frac{3}{2}$ for Na^{23}, the Zeeman Hamiltonian yields four energy levels spaced equally by an amount $\hbar\omega_0$.

When the Ag^+ ion is substituted for the Na^+ ion, the lattice relaxes about the impurity destroying the cubic and inversion symmetries of the rare

nuclei, the near-neighbor nuclei. As a result, the EFG's are nonzero at the rare nuclear sites with a resulting quadrupole splitting of the Zeeman energy levels.

An external oscillating electric field modulates the relative positions between the nuclei in the lattice creating time-dependent EFG's at the nuclear sites. As a result, electric spin transition of $\Delta m = \pm 1$ and $\Delta m = \pm 2$ can be induced. However, because of the difference in inversion symmetry between the rare and abundant nuclei, the behavior of the two species is vastly different.

Consider the electric field to be oscillating at $2\omega_0 + \omega_Q$. For the abundant nuclei, inversion symmetry implies that the electric field gradient (EFG) must vary quadratically with displacement. Since displacement is proportional to the electric field E, the EFG's oscillate at a frequency of $4\omega_0 + 2\omega_Q$. Not only would the transition rate be second order and thus weak, but there are no energy levels with spacings of $4\omega_0 + 2\omega_Q$ and thus no transitions are induced. For the rare nuclei, since inversion symmetry has been destroyed, the EFG's vary linearly with displacement and therefore oscillate with a frequency $2\omega_0 + \omega_Q$. Transitions of $\Delta m = \pm 2$, between the $-\frac{3}{2}$ and $+\frac{1}{2}$ levels are induced. Thus the symmetry selection rule is explained.

An electric field frequency of $\omega_0 + \omega_Q$ was not applied since it was expected that the inevitable stray magnetic fields would still dominate the energy absorption.

Experiments that have observed quadrupole splittings as a function of an applied dc electric field have been done on Ga^{69}, Ga^{71}, and As^{75} nuclei in $GaAs$[12] and on the I^{127} nucleus in KI.[13] In both cases for $E = 0$, the quadrupole splittings are zero, but in GaAs the nuclear sites lack inversion symmetry, whereas in KI the I^{127} nucleus is at a site of inversion symmetry. In GaAs, electric fields on the order of 20 kV/cm yielded easily observable quadrupole splittings that varied linearly in E. However, in KI no quadrupole splitting was observed although an electric field of 50 kV/cm was applied. These results give strong experimental foundation to the assumption of a symmetry selection rule in the EFDOR experiment. They also remind us that though the electric field gradient may be small (even zero), it may still have a change linear in E.

It must be emphasized that by virtue of the symmetry selection rule, the electric field coupling is expected to decrease rapidly as a function of distance from the impurity site, a fact verified experimentally.

In the EFDOR experiment the energy levels of the rare and abundant spins are essentially the same since the near-neighbor quadrupole line in question is under or close to the main line. It is just that line position that makes the $standard$

PNMDR experiment ineffective but ensures the
success of the EFDOR experiment since the rare
and abundant spins are in good thermal contact.

This good thermal contact yields the possibility
of an enhanced sensitivity to the rare spins when
compared to the sensitivity of direct observation.
Consider the electric field to saturate the rare
spins, which, because of good thermal contact,
come into thermal equilibrium with the abundant
spins. This one cycle occurs in a characteristic
time τ. The initial and final abundant-spin mag-
netizations for one cycle are

$$M_s/M_i = 1/(1+\epsilon),$$

where ϵ is the ratio of the heat capacities of the
rare spins to the abundant spins. For identical
spins with approximately equal energy-level spac-
ings, $\epsilon \sim c_{eff}$, where c_{eff} is the effective concen-
tration of sodium nuclei excited by the electric
field. For N such mixing cycles,

$$\frac{M_f}{M_i} \cong \left(\frac{1}{1+c_{eff}}\right)^N \simeq e^{-Nc_{eff}}$$

for small c_{eff}, where

$$N = T_1/\tau .$$

Thus, for $T_1 > \tau$, the sensitivity of direct observa-
tion is increased by N, the enhancement factor.

The characteristic time τ is the sum of the cross-
relaxation time τ_{cr}, the spin-diffusion time τ_{sd}, and
the electric field interaction time τ_E. In the case
where there is no spin-diffusion bottleneck, for
$\tau_E > \tau_{cr}$ the enhancement factor is T_1/τ_E. However,
if $\tau_{cr} > \tau_E$, a cross-relaxation bottleneck occurs
and the enhancement factor becomes T_1/τ_{cr}.

B. Experimental Procedure and Apparatus

The experiment was done at liquid-nitrogen tem-
perature 77 °K giving a T_1 of 400 sec. In order to
decrease the dependence on gain stability, a 90°-
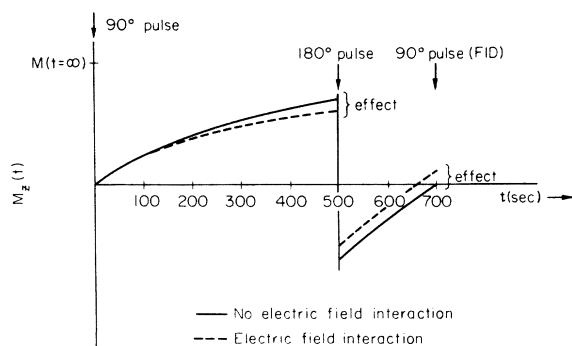180°-90° pulse sequence, shown in Fig. 2, was

FIG. 2. Magnetization as a function of time during the
90-180°-90° pulse sequence.

used so that a null was obtained in the absence of
the effect. However, in order to obtain a stable
null, the pulse sequence was timed by counting a
10-MHz crystal clock.

rf phase sensitive detection was used for the
measurement of the free-induction decay (FID)
which followed the 90° pulse. The FID was inte-
grated and recorded on a digital double boxcar.
The receiver coil was solenoidal and was connected
to a receiver multiplex box via 3 ft of Microdot
cable. In the box were two capacitors in series
connected across the cable. One capacitor was
~ 500 pF and the other ~ 50 pF. These were ad-
justed so that the receiver-coil circuit was tuned
at 10.5 MHz and so that the large capacitor was
at 50 Ω in order to match the 50-Ω input of the
Varian receiver.

In order to obtain an H_1 of 30 G at low input
power, the receiver coil also served as the trans-
mitter coil. Crossed diodes in series with the
transmitter and crossed diodes in parallel with the
receiver protected the receiver during H_1 pulses
and isolated the low-Q transmitter circuit from
the receiver during the FID measurement.

The samples were grown by Spencer and are
described in his paper.[2] The sample holder was
a cylinder, with a $\frac{1}{2}$-in. diam and about a 1-in.
length. In it was placed the sample which was
cleaved in the $\langle 100 \rangle$ direction. A hole was drilled
between the windings of the receiver coil so that
the face of the crystal would be seen through the
slits of the nitrogen Dewar. Since the quadrupole
spectrum is a sensitive function of angle, it is
necessary to know the angle of the crystal axis
with respect to $\vec{H}_0$ reasonably well.

Alignment was accomplished optically as follows.
A split prism was positioned in the magnet gap by a
spacer between it and the magnet pole face, so that
one prism face was accurately parallel to the mag-
net pole face, and the prism was approximately the
same distance from the pole face as the sample
crystal. A laser beam was aimed at the split prism
from outside the magnet gap. The laser was po-
sitioned and aimed so that its beam was approxi-
mately parallel to the magnet face. The prism
divided the beam. One portion reflected from the
prism interface, making nearly a 90° turn, hit the
magnet face, was reflected back to the prism, was
turned again through roughly 90°, and emerged from
the gap heading almost back towards the laser. The
other beam passed through the prism, hit the sam-
ple crystal, was reflected back through the prism,
and also emerged from the gap nearly at the laser.
If the sample were turned until the two emergent
beams coincided, the exposed sample face was nor-
mal to the magnet face. The angle could be deter-
mined to within $\pm \frac{1}{3}°$. For this orientation θ was
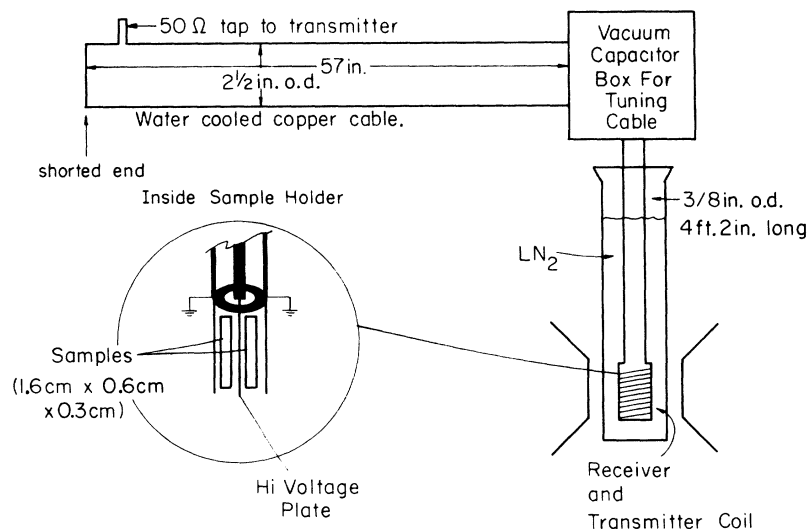defined as zero.

FIG. 3. Oscillating electric field circuit.

Developing a large voltage across the sample at 21 MHz was accomplished by employing a shorted quarter-wavelength cable, shown in Fig. 3, with the sample placed at the infinite impedance end. A 300-W cw transmitter was connected to the cable via a 50-Ω cable to a 50-Ω tap built into the cable. A motorized vacuum capacitor, connected in parallel with the cable just outside the Dewar, was used as the tuning element. A standing-wave radio meter was connected in series between the transmitter and the 50-Ω tap. Obtaining a minimum in reflected power by varying the capacitor indicated that the cable was tuned.

The high-power and high-rf electric field created heating and voltage-breakdown problems. Since the shorted end of the cable carried a great deal of current, the cable had to be water cooled to prevent tuning drift. All cables were fabricated using Teflon spacers to minimize rf heating from the electric fields. An Emerson and Cuming product, Eccomax HI-Q, a low-loss epoxy that is easily machined, was used. To obtain as high an electric field as possible, the sample was cleaved into two pieces, approximately $1.6 \times 0.6 \times 0.3$ cm each. A center plate of 0.03-in. copper, with all edges smoothed, served as the high-voltage plate and copper foil on the outside crystal faces served as ground. Teflon spacers of 0.01 in. were properly placed in the sample holder to prevent voltage breakdown, a configuration allowing about 5 kV/cm to be generated.

Because of the close proximity of the receiver coil and the high-voltage plate, the receiver coil was weakly coupled to the electric field. The induced voltage was used to monitor the electric field. During the electric-field irradiation, a coaxial relay switched the receiver cable to a monitor circuit consisting of a diode and a capacitor with a digital voltmeter for measuring the resulting dc voltage. The electric field voltage could be maintained to within $\pm 1\%$ for the duration of the experiment, limiting the signal-to-noise ratio to 50:1.

III. THEORY AND EXPERIMENTAL RESULTS

A. Quadrupole Spectrum

The rotation of the crystal was about the $\langle 010 \rangle$ axis so that $\vec{H}_0$ rotates in the $\{100\}$–$\{001\}$ plane. For $\vec{H}_0$ along the $\langle 001 \rangle$ direction, $\theta \equiv 0°$.

Using the symmetry arguments for the nuclear sites discussed by Anderson and Forslind,[14] the quadrupole spectrum for the first shell of sodium nuclei is given in Table I.

Since the directions of the principal axes of the field-gradient tensor are known, only one rotation about a crystalline axis is needed to completely determine η and ν_Q,[15] if indeed the first shell is observed.

Although the (2, 2, 0) nuclei have the same angular pattern as the (1, 1, 0) nuclei, the spectrum is attributed to the latter, since it is judged unlikely that the (2, 2, 0) nucleus would have both static and dynamic quadrupole coupling larger than the (1, 1, 0) nucleus.

TABLE I. First-shell quadrupole splittings as a function of angle.

Na[23] sites	Predicted quadrupole splittings
$(\pm 1,\ 0,\ \pm 1)$	$\nu_{101} = \pm (\tfrac{1}{4}\nu_Q)\{(1 + \eta) - (3 - \eta)\ \sin 2\theta\}$
$(\pm 1,\ 0,\ \mp 1)$	$\nu_{101} = \pm (\tfrac{1}{4}\nu_Q)\{(1 + \eta) + (3 - \eta)\ \sin 2\theta\}$
$(\pm 1,\ \pm 1,\ 0)\ (\pm 1,\ \mp 1,\ 0)$	$\nu_{110} = \mp (\tfrac{1}{8}\nu_Q)(1 + \eta)\ \{1 + 3\ \cos 2\theta\}$
$(0,\ \pm 1,\ \pm 1)\ (0,\ \pm 1,\ \mp 1)$	$\nu_{011} = \mp (\tfrac{1}{8}\nu_Q)(1 + \eta)\ \{1 - 3\ \cos 2\theta\}$

B. Quadrupole Line Intensity

Abragani[16] has derived a formula for the magnetization as a function of time for NaCl when irradiated by ultrasonic waves at twice the Larmor frequency. In his derivation he assumed that: the spin-lattice-relaxation mechanism can be described by a single spin-lattice-relaxation time T_1; the spin-spin interaction maintains a Boltzmann distribution between population levels. Thus, he derived the result

$$\frac{d\langle I_z \rangle}{dt} = -\frac{\langle I_z \rangle - I_0}{T_1} - \tfrac{8}{5} A \langle I_z \rangle , \tag{1}$$

where A is the transition probability per unit time for $\Delta m = \pm 2$ transitions.

This equation is valid for our experiment, provided that the cross-relaxation time τ_{cr} is sufficiently short and the fact that only a small number of nuclei are being excited is taken into account. Thus, for $M_z \propto \langle I_z \rangle$,

$$\frac{dM_z}{dt} = -\frac{M_z - M_0}{T_1} - \frac{M_z}{T_E} , \tag{2a}$$

where

$$T_E \equiv \frac{5}{8A} \equiv \frac{5}{8\Gamma_E C_{eff}} . \tag{2b}$$

Γ_E is the transition rate induced by the electric field. Solving for $M_z(t)$, for $T_E \gg T_1$, at any time t_1, the relative destruction of magnetization caused by the electric field is

$$\Delta M/M = -T_1/T_E . \tag{3a}$$

Since $T_E \propto E^{-2}$,

$$\Delta M/M \propto E^2 . \tag{3b}$$

Again, this is valid only if $T_E \gg T_1$ and $\tau_{cr} \ll \tau_E$.

The relative intensities of the quadrupole lines in a standard PNMDR experiment depend on the type of transition induced and the number of equivalent nuclear sites. In addition, as a result of the fourfold symmetry of the NaCl lattice about the $\langle 010 \rangle$ direction, all of the quadrupole spectra information is contained between $\theta = 0°$ and $\theta = 45°$, since the spectra are identical for θ and $90° - \theta$.

This is not the case in EFDOR, since the values of the matrix elements that contribute to $\Delta m = \pm 2$ transitions also depend on the angle between E and H_0. In this experiment the electric field is fixed with respect to the crystal. By symmetry one can see that there is twofold symmetry of E with respect to H_0. Therefore, all the quadrupole line intensity information must be contained between $\theta = 0°$ and $90°$. Although the quadrupole *splittings* of the spectra of $\theta = 0°$ and $\theta = 90°$ are identical, the quadrupole *spectra* should be different since the relative line intensities are different.

To explain the relative intensities of the quadrupole lines, a simple model based on symmetry arguments will be presented. Since the silver ion and sodium ion interact differently with the lattice, the application of the electric field must cause the silver ion to have a displacement relative to the sodium fcc lattice. Figure 4(a) illustrates the relative motion of the silver ion with respect to the (1, 0, 1) sodium site, with the electric field in the $\langle 100 \rangle$ direction. Figure 4(b) shows the components of the motion along the vector (called the radius vector) directed from the equilibrium position of
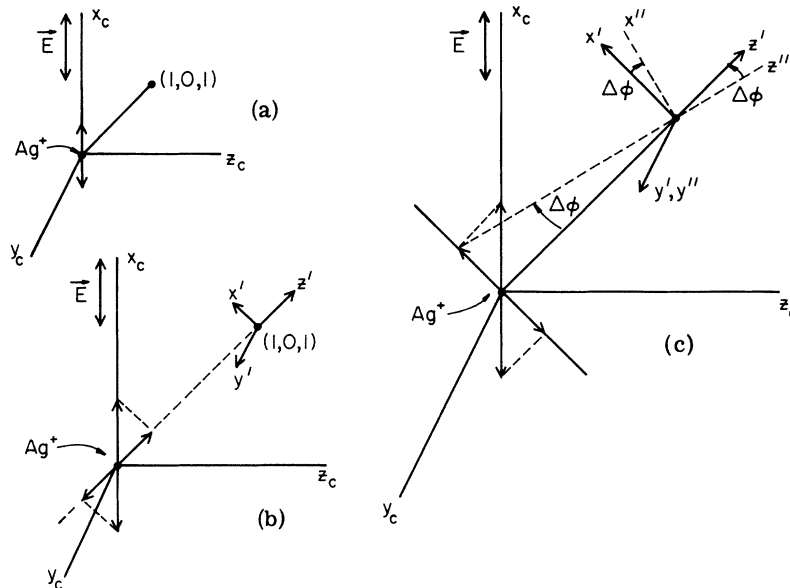

FIG. 4. (a) Relative motion of the Ag⁺ with respect to the (1, 0, 1) Na⁺ site. The subscript c denotes crystal axes. (b) Component of the relative motion along the radius vector. (c) Component of the relative motion perpendicular to the vector.

the silver ion to the (1, 0, 1) site. Figure 4(c) shows the component of the motion that is perpendicular to the radius vector. Note that the x', y', z' axes shown are the same as the principal axes of the static EFG tensor.

In order to establish which elements in the EFG tensor change linearly in E, consider Fig. 4(c), in which the components perpendicular to the radius vector are shown. The effect of the motion of this component can best be visualized by considering an x'', y'', z'' coordinate system, rotating about the y', y'' axes by an amount $\Delta\phi$, where $\Delta\phi \propto E$. The rotation is such that the z'' axis *approximately* follows the silver ion. In the double primed axes, by symmetry, whatever change in EFG that might exist must be the same for $\pm\Delta\phi$. Thus in the double-primed system there is no change in EFG to first order in E. In transforming from the double-primed system to the primed system, by symmetry, there can be no first-order change in E in the y direction. Defining

$$V'_{x'y'} = \frac{\partial V_{x'y'}}{\partial E} ,$$

we see that $V'_{x'y'}$, $V'_{y'y'}$, $V'_{y'z'}$ are zero. The components $V'_{x'x'}$ and $V'_{z'z'}$ transform as $\cos\Delta\phi$ and thus only possess second-order variation in E. The only term that transforms in first order in E is the $V'_{x'z'}$ term. For the motion in the radius vector direction, symmetry dictates that only the $V'_{x'x'}$, $V'_{y'y'}$, and $V'_{z'z'}$ terms should be nonzero. So for the $(\pm 1, \pm 1, 0)$, $(\pm 1, \mp 1, 0)$, $(\pm 1, 0, \mp 1)$, and $(\pm 1, 0, \pm 1)$ nuclei,

$$V'_{\alpha'\beta'} = \begin{Vmatrix} \alpha_{x'} & 0 & V \\ 0 & \alpha_{y'} & 0 \\ V & 0 & \alpha_{z'} \end{Vmatrix} \frac{E}{\sqrt{2}} ,$$

where V, $\alpha_{x'}$, $\alpha_{y'}$, $\alpha_{z'}$ are constants; $E/\sqrt{2}$ is the component of the electric field along and perpendicular to the radius vector. By Laplace's equation

$$\alpha_{x'} + \alpha_{y'} + \alpha_{z'} = 0 .$$

Note that this tensor must be constructed at the nuclear sites with the x', y', z' axes shown in Fig. 4. Defining a dynamic asymmetry parameter

$$\eta_D = (\alpha_{x'} - \alpha_{y'})/\alpha_{z'}$$

and a constant R that yields the relative strengths of the two motions

$$R \equiv \alpha_{x'}/V ,$$

the two parameters R and η_D completely define the tensor.

For the (0, 1, 1) nucleus the electric field only moves the silver nucleus perpendicular to the radius vector from the Ag$^+$ equilibrium point to the (0, 1, 1) site. The relationship of the perpendicular motion to the nearest-neighbor chlorine ions for the (0, 1, 1) Na$^+$ ion is different from the similar

relationship for the other first-shell Na$^+$ sites. Although the mechanism is the same, the value of the tensor component must be different. Assigning the proper $x'y'z'$ axes, the only nonzero tensor element is $V'_{y'z'} = V_1$.

For the (2, 0, 0) nucleus one can easily see that the only nonzero terms are $V'_{x'x'}$, $V'_{y'y'}$, and $V'_{z'z'}$, where $V'_{x'x'} = V'_{y'y'} = -2V_{z'z'} = -2V_2$. Likewise, for the (0, 0, 2) and (0, 2, 0) nuclei the only nonzero tensor element is $V'_{x'z'} = V_3$.

In order to obtain the intensities as a function of angle, the same transformation that was used to find the rotation patterns are also used to find the relative intensities as a function of angle. The square of the matrix elements of the various lattice positions are given in Table II. The subscripts on M denote the nuclear site. Each expression has taken into account the number of equivalent nuclei contributing to the intensity; $B_1 = (\frac{1}{2}R)(\eta_D + 1) - 2$, $B_2 = B_1 + 4$, $B_3 = \frac{1}{2}(3 - \eta_D)R$, $B_4 = -R(\eta_D + 1)$, $\mu = \cos\theta$, $\xi = \sin\theta$, and $D = \frac{1}{12}eQ$.

C. Data and Comparison to Theory

In addition to the two parameters ν_Q and η that define the static quadrupole splittings as a function of angle, the intensity parameters for the first shell V, V_1, η_D, and R and the intensity parameters for the second shell V_2 and V_3 must be determined. Mallick and Schumacher[1] have measured $\nu_Q = 40$ kHz and $\eta = 0$ for the second shell.

The parameters η and ν_Q for the first shell and the parameters for describing the relative intensities of the first shell were determined by comparing computer generated spectra to the data for $\theta = 0°$, $90°$, $85°$, $80°$, $70°$, $65°$, and $55°$ for $E = 1.1$ kV/cm. Inspection of the data determined that $V_1 = V_3 = 0$ (the reason behind these choices will be discussed shortly). As a result of these choices, only η_D and R had to be determined for the relative intensities of the first shell since the parameter V was then only a multiplicative factor to be determined by the actual value of the destruction of magnetization. Gaussian lines were used with a half-width at half-height defined to be σ. Thus, first

TABLE II. Electric field interaction matrix elements for first- and second-shell sodium nuclear sites.

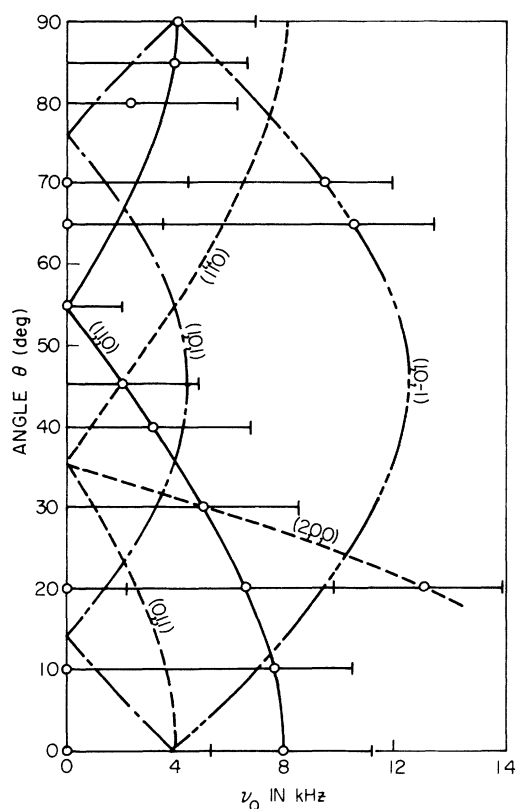| Matrix element	Function
$\|M_{101}\|^2$	$\frac{1}{16}(V^2D^2E^2)\{B_2\mu^2 + B_1\xi^2 + 2B_3\mu\xi - B_4\}^2$
$\|M_{10-1}\|^2$	$\frac{1}{16}(V^2D^2E^2)\{B_2\mu^2 + B_1\xi^2 + 2B_3\mu\xi - B_4\}^2$
$\|M_{110}\|^2$	$\frac{1}{8}(V^2D^2E^2)\{B_2\mu^2 + B_4\xi^2 - B_1\}^2 + \frac{1}{2}(V^2D^2E^2)B_3^2\mu^2$
$\|M_{011}\|^2$	$16 D^2V_1^2\mu^2\xi^2 + 4D^2E^2V_1^2\mu^2$
$\|M_{200}\|^2$	$\frac{9}{2}V_2^2D^2E^2\mu^4$
$\|M_{002}\|^2$	$2 D^2V_3^2E^2\mu^2\xi^2$
$\|M_{020}\|^2$	$2 D^2V_3^2E^2\mu^2$

FIG. 5. Quadrupole splittings as a function of angle
for the first and second shells of Na nuclei in NaCl : Ag.

shell spectra were generated for various values of
ν_Q, η, η_D, R, and σ until the best fit was obtained.

The best values for the first shell are $\eta_D = 0.60$
± 0.05, $R = -0.60 \pm 0.05$, $\nu_Q = 12.5 \pm 0.2$ kHz, η
$= 0.28 \pm 0.04$, and $\sigma = 2.3 \pm 0.1$ kHz.

Figure 5 is a theoretical plot of the quadrupole
splittings for the first and second shells as a func-
tion of θ. The circles drawn on the plot designate
identifiable peaks in the data and line edges are
represented by error bars. This figure is a sum-
mary of the data and theory.

Upon comparing the data to the theoretical be-
havior expected of the first shell, two factors must
be kept in mind. First, since the (0, 1, 1) nucleus
was not seen in the theoretical plot, it was as-
sumed that the (0, 1, 1) nucleus has a small dynamic
coupling constant with the electric field along the
$\langle 100 \rangle$ direction, thus $V_1 = 0$. Second, because the
remaining three lines of the first shell are crowded
into a small frequency range of 12 kHz, first- ver-
sus second-order changes of line positions and
widths with angle, as well as line positions as a
function of angle, become important features.

Figure 6 is a plot of the data points and theoret-
ical fits at $\theta = 90°$ and $\theta = 0°$ for $E = 1.1$ kV/cm.
They differ because the experiment has twofold
rather than fourfold symmetry. Figure 7 is a plot
of the curves and theoretical fits at $\theta = 90°$, $80°$,
$70°$, and $55°$ at $E = 1.1$ kV/cm. We conclude that
the theoretical curves are a reasonably good fit to
the data. Upon examination of the fit and the data
we see that the assumption that $V_1 = 0$ may not be
exact. However, since the (0, 0, 2) nucleus is not
seen, i.e., $V_3 = 0$, and since the (0, 1, 1) and (0, 0, 2)
nuclei both have the same relative position with
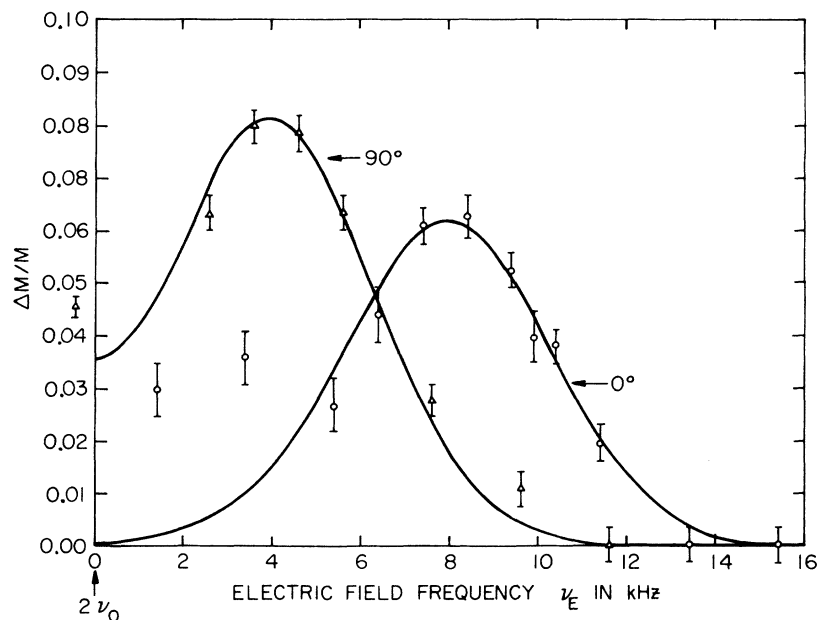respect to the electric field, there is internal con-

FIG. 6. Data and com-
puter generated spectra
for $\theta = 0°$ and $\theta = 90°$. E
$= 1.1$ kV/cm; O = 0° and
$\Delta = 90°$.
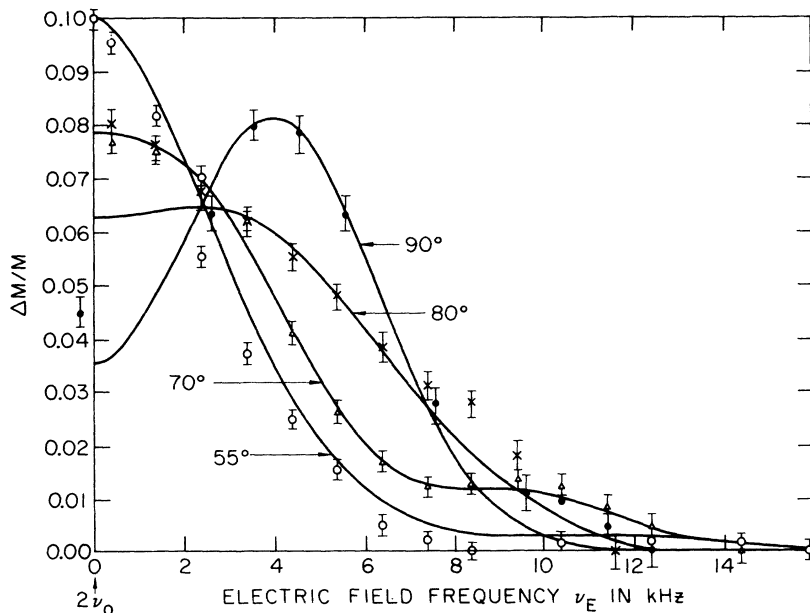
FIG. 7. Data and computer generated spectra for $\theta = 90°$, $80°$, $70°$, and $55°$; $E = 1.1$ kV/cm.

sistency in assuming $V_3 = V_1 = 0$.

Figure 8 contains the rotation pattern for $\theta = 55°$, $\theta = 45°$, $\theta = 40°$, and $\theta = 30°$. The curves taken at $45°$, $40°$, and $30°$ were taken at an electric field of $E = 4.5$ kV/cm, a power level of four times the level for the $90°-55°$ curves. Initially, data taken between $0°$ and $45°$ were taken at this higher level in order to obtain as much destruction as possible for good signal to noise. However, it was discovered that the cross-relaxation bottleneck distorted the spectrum at those high-field levels (direct evidence of this problem will be shown shortly). At $E = 1.1$

kV/cm there is no observable cross-relaxation bottleneck. No low-field data ($E = 1.1$ kV/cm) between $\theta = 0°$ and $45°$ were taken. However, the $45°$ and $40°$ spectra can still be compared to the $55°$ spectrum because the general features of the two curves are correct. The theory predicts that if the $(1, 1, 0)$ line is strong, and the $(0, 1, 1)$ line is weak, the spectrum should exhibit a first-order change in width as θ goes from $55°$ to $40°$. This behavior is quite obvious in Fig. 8.

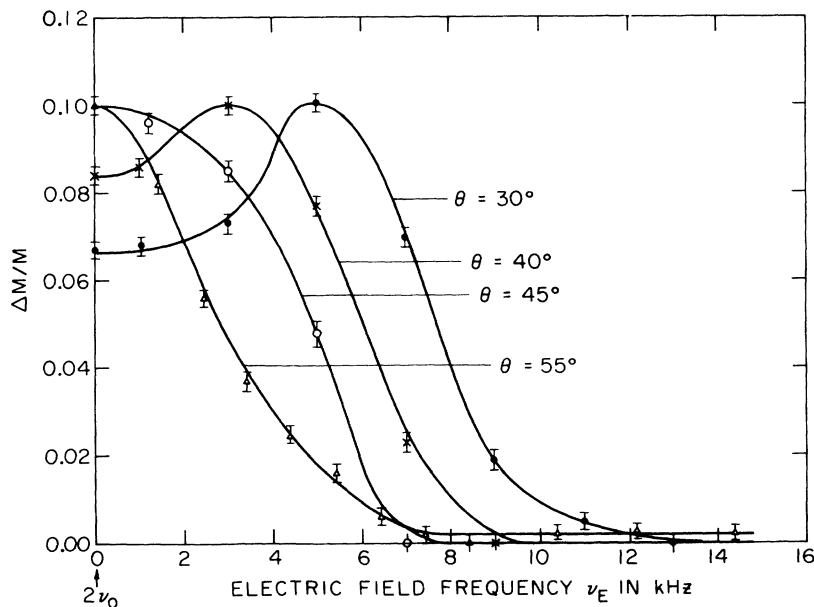Figure 9 shows the data for $\theta = 0°$, $10°$, and $20°$ for $E = 4.5$ kV/cm. For $\theta = 20°$ the $(2, 0, 0)$ line is

FIG. 8. Data taken at $\theta = 55°$ for $E = 1.1$ kV/cm and at $\theta = 45°$, $40°$, and $30°$ for $E = 4.5$ kV/cm. The data are normalized to 0.1. $\triangle = 55°$, $O = 45°$, $\times = 40°$, $\bullet = 30°$.
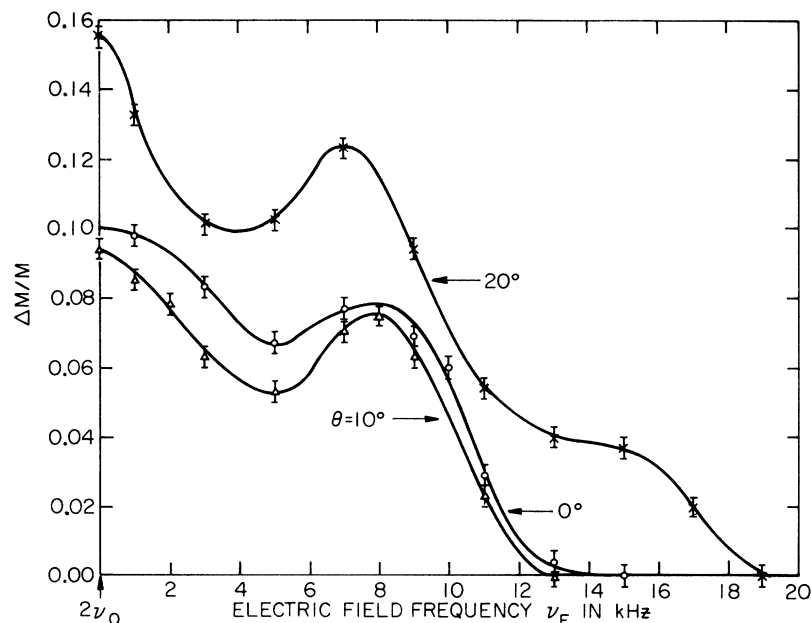
at 13 kHz.[1,2] This line is evident for $\theta = 20^\vee$ in Fig. 9.

All the features mentioned up to now are summarized in Fig. 5. Taking this summary along with the reasonably good theoretical fit for $\theta = 0°$, 90°, 85°, 80°, 70°, 65°, and 55°, we conclude that the first and second shells of sodium nuclei have been observed and that the simple model explains the relative intensities.

Direct evidence of the cross-relaxation bottleneck can be seen in Fig. 10, in which a log-log plot of the relative destruction of magnetization as a function of electric field measured at $\theta = 0$ for $\nu = 8$ and 0 kHz and at $\theta = 20°$ for $\nu_E = 14$ kHz is shown. Note the E^2 dependence in both cases. For the electric field available it was possible to create a cross-relaxation bottleneck at 8 kHz but not at 0 kHz. At $E = 4.5$ kV/cm the 8-kHz line is about 70%
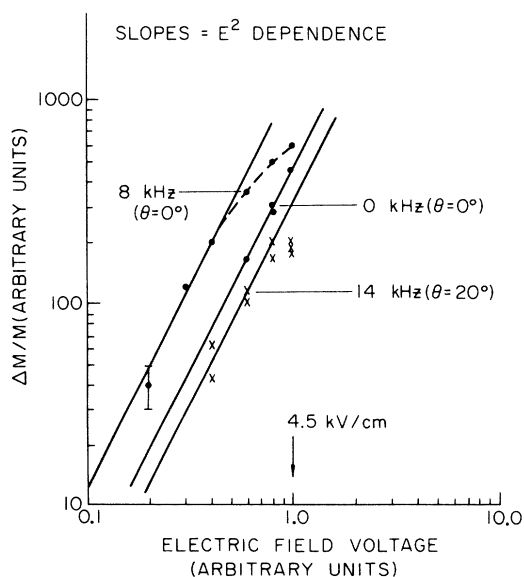

FIG. 10. log-log plot of the relative destruction of magnetization as a function of electric field taken at $\nu = 0$ and $\nu = 8$ kHz for $\theta = 0°$ and at $\nu = 14$ kHz for $\theta = 20°$.
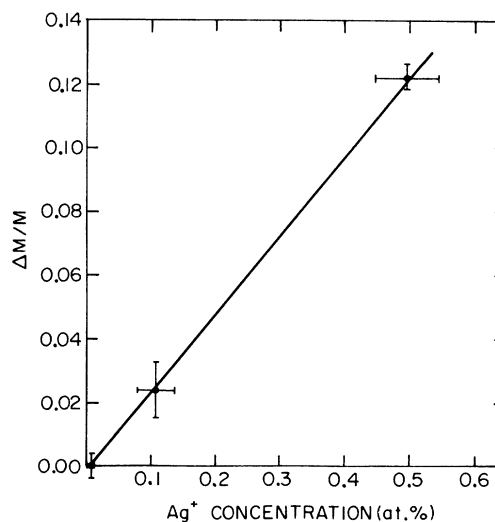

FIG. 11. Intensity of the 7-kHz peak for $\theta = 20°$ as a function of concentration. Horizontal bars include uncertainty of concentration and absolute value of E. Vertical bars include limitations in signal to noise and uncertainty in angle.

TABLE III. Experimental values for $R_{\alpha'\beta'\gamma'}$.

Nucleus	Material	$R_{ijk} \times 10^9$ cm^{-1}	Ref.
Ga^{69}	GaAs	$R_{123} = 10.5$	12
Ga^{71}	GaAs	$R_{123} = 9.0$	12
As^{75}	GaAs	$R_{123} = 15.5$	12
Cl^{35}	NaClO$_3$	$R_{333} = 2.1$	17
Cl^{35}	CCl$_4$	$R_{333} = 5.0$	18
Al^{27}	Al$_2$O$_3$	$R_{333} = -2.9$	19

smaller than it would be with no cross-relaxation bottleneck. Figure 11 shows that as expected the destruction of magnetization varies linearly with concentration. The intensity of the 7-kHz peak at $\theta = 20°$ is plotted as a function of concentration for 0.007-, 0.11-, and 0.5-at.% Ag$^+$.

At $\theta = 55°$, the strong (1, 1, 0) nucleus has zero quadrupole splitting. It is the main contributor to the destruction of magnetization which is $10\% \pm 1\%$. Since at $\nu = 0$ there is no cross-relaxation problem, for small destruction

$$\Delta M/M = 0.1 \quad . \tag{4}$$

Thus, using the measured T_1 and Eq. (3a),

$$T_E = 4000 \text{ sec.} \tag{5}$$

For a perfectly homogeneous sample, $c_{eff} = 0.02$, thus Eq. (3b) becomes

$$\Gamma_E = 8 \times 10^{-3} \text{ sec}^{-1} \quad . \tag{6}$$

Assuming negligible saturation and Lorentzian lines,

$$\Gamma_E \sim (2 T_2/\hbar^2)|\langle M \rangle|^2 \quad . \tag{7}$$

Defining a dynamic quadrupole coupling constant as

$$\nu_D \equiv eQV/2h \tag{8}$$

and equating Eqs. (6) and (7),

$$\nu_D^{(1)} \sim 3 \times 10^{-2} \text{ Hz/(V/cm)} \tag{9}$$

for the first shell. Similarly,

$$\nu_D^{(2)} \sim 3 \times 10^{-3} \text{ Hz/(V/cm)}$$

for the second shell.

With this value for ν_D, the electrically induced transition rate for 1 V/cm is

$$\Gamma_E \sim 3 \times 10^{-7} \text{ sec}^{-1}$$

for the first shell. Kushida and Silver[11] found that the electrically induced transition probability for $\Delta m = \pm 2$ transition in Al^{27} in Al$_2$O$_3$ was 1.5×10^{-7} Hz/(V/cm). In addition, Luukkala[10] observed the transition rate in Na^{23} in NaClO$_3$ to be on the order of 10^{-8} Hz/(V/cm). Although there is no basis for direct comparison of these values, their proximity implies that the experimental value of Γ_E is reasonable.

A third rank tensor $T_{\alpha'\beta'\gamma'}$ can be defined such that the change in quadrupole frequency $\Delta\nu_{\alpha\beta}$,

$$\Delta\nu_{\alpha'\beta'} = \nu_D \sum_{\gamma'} T_{\alpha'\beta'\gamma'} E_{\gamma'} \quad , \tag{10}$$

where γ' is summed over $x'y'x'$, the principal axes of the static electric-field-gradient tensor. Equation (10) can be used as a second check on the order of magnitude of ν_D by comparing its value to the induced quadrupole splitting caused by a static electric field in a linear Stark experiment.[12,17-19] In these experiments a third-rank tensor $R_{\alpha'\beta'\gamma'}$ is defined such that

$$\Delta(eq)_{\alpha'\beta'}^E = \sum_{\gamma'} R_{\alpha'\beta'\gamma'} E_{\gamma} \quad , \tag{11}$$

where $\Delta(eq)_{\alpha'\beta'}^E$ is the change in field gradient caused by the electric field. Table III gives a summary of some typical values of R_{ijk} for the various experiments.

Except for the fact that ν_D is defined in the context of a time-varying electric field, one would expect a reasonable order of magnitude agreement. Multiplying Eq. (10) by $2h/eQ$ and comparing the result to Eq. (11), for $\alpha' = \gamma' = x' = 1$, and $\beta' = z' = 3$,

$$R_{131} \sim \nu_D T_{131} 2h/eQ \quad .$$

Taking $1 - \gamma_\infty$ to be 5.5,[20] where γ_∞ is the Sternheimer antishielding factor, the data yield

$$R_{131} \sim 3.7 \times 10^8 \text{ cm}^{-1} \quad ,$$

which compares favorably with Table III.

IV. SUMMARY AND CONCLUSIONS

The first and second shells of sodium nuclei in NaCl:Ag$^+$ have been observed by the EFDOR technique. $\nu_Q = 12.5 \pm 0.2$ kHz for the first shell proves the assumption that the quadrupole coupling is smaller for the first shell than for the second shell. The asymmetry parameter for the first shell is $\eta = 0.28 \pm 0.04$. The quadrupole lines are approximately gaussian with the half-width at half-height of 2.3 ± 0.1 kHz.

A theory, developed to explain the relative intensities of the quadrupole lines, was reasonably successful. The dynamic quadrupole coupling constant for the first shell is $\nu_D = 3 \times 10^{-2}$ Hz/(V/cm) and for the second shell is $\nu_D = 3 \times 10^{-3}$ Hz/(V/cm). The cross-relaxation bottleneck was demonstrated.

The EFDOR technique presented here should work for defect problems, in general, provided that the sample has the proper symmetry. It complements the standard NMDR technique by allowing observation of spectra under the main line.

†Research supported in part by the U. S. Atomic Energy Commission, under Contract No. AT(11-1)-1198.

*Present address: Sandia Laboratories, Albuquerque, N. M. 87115. This paper is based on the Ph. D. thesis presented by Dr. Meyer at The University of Illinois.

‡Present address: Bell Laboratories, Murray Hill, N. J. 07971.

[1] G. T. Mallick, Jr. and R. T. Schumacher, Phys. Rev. 166, 350 (1968).

[2] P. R. Spencer, H. D. Schmid, and C. P. Slichter, Phys. Rev. B 1, 2989 (1970).

[3] K. F. Nelson and W. D. Ohlsen, Phys. Rev. 180, 366 (1969).

[4] M. Satoh, P. R. Spencer, and C. P. Slichter, J. Phys. Soc. Jap. 22, 666 (1967).

[5] A. Hartland, Proc. Roy. Soc. Lond. A 304, 361 (1968).

[6] B. G. Dick, Phys. Rev. 145, 609 (1966).

[7] N. Bloembergen, Science 133, 1363 (1961).

[8] J. Armstrong, N. Bloembergen, and D. Gill, Phys. Rev Lett. 7, 11 (1961).

[9] E. Brun, R. Hann, W. Pierce, and W. H. Tanttila,

Phys. Rev. Lett. 8, 365 (1962).

[10] M. Luukkala, Phys. Lett. 10, 20 (1964).

[11] T. Kushida and W. H. Silver, Phys. Rev. 130, 1692 (1963).

[12] D. Gill and N. Bloembergen, Phys. Rev. 129, 2398 (1963).

[13] R. V. Pound, Phys. Rev. 79, 685 (1950).

[14] L. O. Anderson and E. Forslind, Ark. Fys. 28, 29 (1964).

[15] M. H. Cohen and F. Reif, in *Solid State Physics*, edited by F. Seitz and D. Turnbull (Academic, New York, 1957), Vol. 5.

[16] A. Abragam, *The Principles of Nuclear Magnetisum* (Oxford U. P., London, 1961).

[17] F. A. Collins and N. Bloembergen, J. Chem. Phys. 40, 3479 (1964).

[18] R. W. Dixon and N. Bloembergen, J. Chem. Phys. 41, 1720 (1964).

[19] R. W. Dixon and N. Bloembergen, Phys. Rev. 135, A1669 (1964).

[20] T. P. Das and R. Bersohn, Phys. Rev. 102, 733 (1956).